Characterisation and structure development of $Ni_{64}Cu_9Fe_8P_{19}$ glass forming alloy at elevated temperatures

K. Ziewiec [a], K. Bryła [a], A. Błachowski [b], K. Ruebenbauer [b,*], J. Przewoźnik [c]

[a] *Institute of Technology, Pedagogical University, PL-30-084 Kraków, ul. Podchorążych 2, Poland*
[b] *Mössbauer Spectroscopy Division, Institute of Physics, Pedagogical University, PL-30-084 Kraków, ul. Podchorążych 2, Poland*
[c] *Solid State Physics Department, Faculty of Physics and Applied Computer Science, AGH University of Science and Technology,
PL-30-059 Kraków, Al. Mickiewicza 30, Poland*

Abstract

Nickel–copper–iron–phosphorus $Ni_{64}Cu_9Fe_8P_{19}$ alloy was prepared using 99.95 wt.% Ni, 99.95 wt.% Cu, 99.95 wt.% Fe and the Ni–P master alloy. The precursors were melted in the arc furnace under argon gettered protective atmosphere. Then the alloy was induction melted in quartz tubes under vacuum (10^{-2} bar) and quenched in water to obtain ingot of 10 mm diameter. The primary microstructure of the ingot was investigated by the use of light microscope. The $Ni_{64}Cu_9Fe_8P_{19}$ alloy was cast using melt spinning. The ribbon in the as cast state was characterised with use of transmission electron microscope (TEM) and X-ray diffraction (XRD). Differential thermal analysis (DTA) of the melt-spun ribbon was made to determine the thermal stability and glass forming ability of the alloy. The pieces of ribbon were heated to different temperatures and annealed during 1 h then characterised with use of the Mössbauer spectroscopy and the X-ray diffraction to see the change of the microstructure after heating to elevated temperatures. It has been found that the devitrification sequence consists of progressive formation of the (Ni, Fe, Cu)$_3$P phase and (Ni, Fe, Cu)-FCC phase. The temperature range of the sequence is determined under isochronal conditions.
© 2006 Elsevier B.V. All rights reserved.

PACS: 71.23.Cq; 87.64.Pj; 61.10.-i

Keywords: Melt spinning; Metallic glass; Thermal stability; Crystallisation; Ability to form glass

1. Introduction

Metallic glasses have been designed recently in many multi-component systems [1–3] and are interesting because of some unique properties, e.g. high elasticity limit and low coercivity. These characteristics, which can be hardly found in crystalline materials, are attractive for practical uses of the structural and functional materials. The characteristics of metallic glasses are strongly temperature dependent. Amorphous metallic alloys often show significant plasticity in the supercooled liquid region. It is reported that it is due to a substantial drop of viscosity by several orders of magnitude [4,5]. This can be potentially used in forming bulk shapes starting from the glassy alloys that are not necessarily the best glass formers [6,7]. Recently, several glassy alloys with a wide supercooled liquid region and substantial glass forming ability were elaborated [8–14]. Unfortunately, the best glass formers with a large supercooled liquid region consist of the expensive precursors. Because of the limited resources and high prices of such constituents as Pd, La, Nd and Zr, applications of metallic glasses with the high glass forming ability are still very restricted. Therefore, more common use of good glass formers lies probably behind cheaper precursors and more accessible elements. On the other hand, analysis of available binary and ternary phase diagrams containing Ni, Cu, Fe and P indicates that especially in compositions where one of the constituents is P there are deep eutectics [15] and in Ni–Cu–Fe–P system good glass forming ability can be expected [12]. The Ni–Cu–Fe–P alloys present also supercooled liquid region [16]. Furthermore, the eutectic alloys or the ones very close to the eutectic show good glass forming ability. Therefore, the present work presents investigation of the $Ni_{64}Cu_9Fe_8P_{19}$ alloy. The latter alloy is very close to the quaternary eutectic alloy. The

paper reports the behaviour of the amorphous $Ni_{64}Cu_9Fe_8P_{19}$ melt-spun alloy during the isothermal heating cycles.

2. Experimental

Nickel–copper–iron–phosphorus $Ni_{64}Cu_9Fe_8P_{19}$ alloy was prepared using 99.95 wt.% Ni, 99.95 wt.% Cu, 99.95 wt.% Fe and the Ni–P master alloy. The precursors were melted in the arc furnace under gettered argon atmosphere. The alloy was remelted five times to assure good mixing of the precursors. After melting at 1050 °C in quartz tubes (10^{-2} bar vacuum) the alloy in capsules was quenched in water. Then the ingot of 10 mm diameter was cut for metallographic observations by means of the light microscope.

Nickel–copper–iron–phosphorus $Ni_{64}Cu_9Fe_8P_{19}$ alloy was melt-spun with 33 m/s linear velocity (approximate cooling rate of 10^5 K/s). The ribbon in the as cast state was preliminarily studied by transmission electron microscope (TEM) and X-ray diffraction (XRD) to find the phase composition. For defining its thermal stability the melt-spun ribbons were investigated by means of differential thermal analysis (DTA). Then, the ribbon in the as cast state was annealed at the following temperatures: 473 K, 573 K, 598 K, 610 K, 623 K, 673 K, and 773 K during 1 h and subjected to Mössbauer and X-ray diffraction studies at ambient temperature after annealing at the above mentioned temperatures.

Some attempts were made to prepare bulk metallic glass (BMG) samples casting the alloy in the water-cooled crucibles having rod-like shapes. It was found that the circumferential parts of the resulting rods are amorphous indeed. However, the present contribution concentrates on the melt-spun samples.

3. Results and discussion

3.1. Transmission electron microscopy

The small area electron diffraction (SAED) pattern of the as cast sample is presented in Fig. 1. The microstructure is uniform and amorphous which is confirmed by the electron diffraction pattern presenting broad diffusive rings. It is interesting to note that the strongest diffraction ring of the Fig. 1 indicates that there is some electron density maximum in the radial correlation function at a distance of about 0.23 nm. This distance
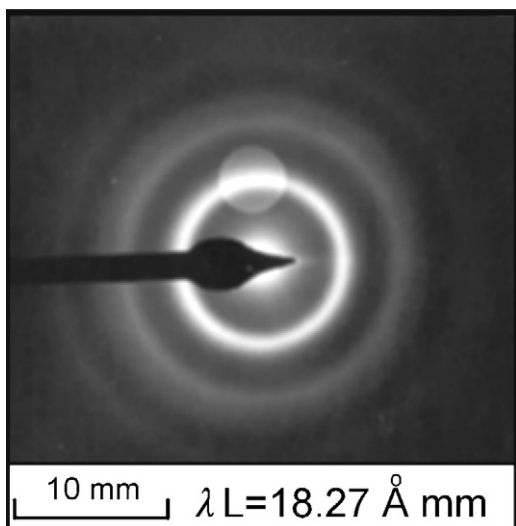

Fig. 1. SAED pattern obtained from the $Ni_{64}Cu_9Fe_8P_{19}$ melt-spun ribbon. The symbol λ stands for the wavelength of the incoming electrons, while the symbol L denotes the distance from the scattering sample to the detector plane, the latter being perpendicular to the incoming beam of electrons. The ghost pattern above the image of the central beam is due to the scattering by the aperture ring and it has nothing to do with the sample investigated.
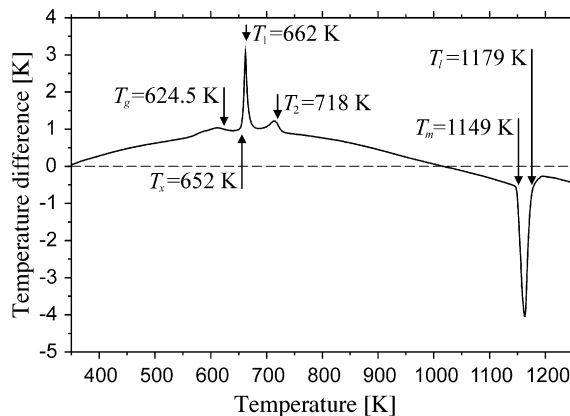

Fig. 2. DTA curve of the $Ni_{64}Cu_9Fe_8P_{19}$ alloy (T_g, glass transition temperature; T_x, the temperature of the onset of the crystallisation; T_1, the first crystallisation peak; T_2, the second crystallisation peak; T_m, melting point; and T_l, liquidus temperature).

is close to the largest metal–phosphorus distance in the crystalline phosphide phase obtained upon crystallisation. It means that metal–phosphorus bonds are similar in the amorphous and crystalline phases.

3.2. Differential thermal analysis

Differential thermal analysis was performed using DTA-STD 2960 TA Instruments setup at the heating rate of 20 K/min. The DTA heating traces of the $Ni_{64}Cu_9Fe_8P_{19}$ alloy are presented in Fig. 2. As it can be seen from the curve the glass transition temperature (middle point) is observed at $T_g = 624.5$ K and crystallisation of the alloy starts at $T_x = 652$ K (crystallisation onset) with the first crystallisation peak at $T_1 = 662$ K and the second crystallisation peak at $T_2 = 718$ K. Further heating of the crystallised alloy leads to melting between $T_m = 1149$ K and $T_l = 1179$ K. Therefore, the investigated alloy presents the supercooled liquid region $\Delta T_x = T_x - T_g$ at the level of 27.5 K. One has to treat the above temperatures determined by means of DTA as approximate due to the fact that DTA is typical non-equilibrium method.

3.3. Mössbauer spectroscopy

Mössbauer spectra were collected at room temperature in the transmission mode. A commercial ^{57}Co(Rh) source was used. Spectra were obtained in a triangular round-corner mirror velocity mode with the help of the MsAa-3 spectrometer [17]. All shifts are reported versus metallic iron at room temperature. Mössbauer spectra are shown in Fig. 3, while the essential results are summarised in Table 1. Fig. 4 shows distributions of the hyperfine magnetic fields.

There are three distinctly different nearest neighbour environments of iron in the amorphous ribbon as cast on the spinning wheel. One of them is characterised by a broad singlet indicating relatively high symmetry around the iron site, while the remaining two are characterised by the non-vanishing electric quadrupole interactions (see, Table 1). The high symmetry site, exhibiting singlet is likely to be similar to the iron environment

Table 1
Essential Mössbauer parameters are listed here

T [K]	Singlet			Doublet 1				Doublet 2			
	c [%]	S [mm/s]	Γ [mm/s]	c [%]	S [mm/s]	Δ [mm/s]	Γ [mm/s]	c [%]	S [mm/s]	Δ [mm/s]	Γ [mm/s]
RT	12	0.18 ± 0.03	0.32 ± 0.34	41	0.24 ± 0.01	0.84 ± 0.06	0.31 ± 0.08	47	0.21 ± 0.01	0.46 ± 0.06	0.30 ± 0.13
473	9	0.17 ± 0.05	0.28 ± 0.50	43	0.23 ± 0.02	0.82 ± 0.06	0.30 ± 0.08	48	0.20 ± 0.01	0.44 ± 0.06	0.30 ± 0.14
573	22	0.17 ± 0.02	0.34 ± 0.27	41	0.26 ± 0.03	0.83 ± 0.07	0.34 ± 0.10	38	0.20 ± 0.02	0.50 ± 0.08	0.31 ± 0.20
598	40	0.14 ± 0.02	0.54 ± 0.20	35	0.26 ± 0.02	0.83 ± 0.07	0.37 ± 0.10	25	0.21 ± 0.04	0.52 ± 0.08	0.35 ± 0.22
610	54	0.14 ± 0.04	0.67 ± 0.20	26	0.28 ± 0.05	0.82 ± 0.22	0.36 ± 0.22	20	0.25 ± 0.09	0.61 ± 0.43	0.36 ± 0.62

T [K]	Singlet			Doublet				Magnetically ordered phase		
	c [%]	S [mm/s]	Γ [mm/s]	c [%]	S [mm/s]	Δ [mm/s]	Γ [mm/s]	c [%]	$<B>$ [T]	$<S>$ [mm/s]
623	12	0.15 ± 0.03	0.56 ± 0.28	12	0.30 ± 0.05	0.89 ± 0.12	0.44 ± 0.20	76	23.80	0.06 ± 0.01
648	7	0.17 ± 0.05	0.42 ± 0.27	19	0.32 ± 0.02	0.82 ± 0.04	0.32 ± 0.08	74	25.24	0.03 ± 0.01
673				42	0.33 ± 0.01	0.78 ± 0.02	0.31 ± 0.03	58	26.20	0.01 ± 0.01
773				46	0.33 ± 0.01	0.77 ± 0.02	0.32 ± 0.04	54	26.38	0.04 ± 0.01

The symbol T stands for the annealing temperature with RT indicating the sample as cast. The symbol c denotes relative contribution of the given iron site to the whole spectrum, S stands for the shift of the particular sub-spectrum (mainly due to the isomer shift) relative to the shift in α-Fe at room temperature and Γ stands for the line-width within particular sub-spectrum. The symbol Δ denotes the absolute value of the quadrupole splitting. On the other hand, the symbol $<S>$ stands for the average shift in the magnetically ordered phase, while the symbol $<B>$ denotes the average hyperfine field on the iron nucleus in this phase.

in the FCC Ni phase with some Fe and Cu dissolved in. However, the isomer shift (0.18 mm/s) indicates that the electron density on the iron nucleus is much lower than in the pure nickel, where the isomer shift was found as −0.05 mm/s [18]. It seems that the low symmetry sites with the quadrupole splittings are those with some phosphorus as the nearest neighbour. The site with the highest splitting has parameters similar to the parameters of the iron in the FeP crystalline phase [19,20]. Therefore, the local environment of iron having none phosphorus as the nearest neighbour is similar in the amorphous phase to the one found later in the crystalline phase containing almost none phosphorus atoms. The iron sites with smaller quadrupole splitting are those depleted in phosphorus neighbours.

Isochronal annealing for 1 h has no effect on the Mössbauer spectra till 473 K. Afterwards a contribution from the high symmetry site increases at the cost of the sites having phosphorus as the nearest neighbours. Particularly the site with less phosphorus as the nearest neighbours transforms into FCC-like site. Such processes are observed in the temperature range 473–598 K for 1-h annealing. The sample annealed at 610 K is characterised by merging of two iron sites having phosphorus as the nearest neighbours. A transformation proceeds towards (Ni, Fe, Cu)P-like site. A contribution from the FCC-like sites is increased in comparison with samples annealed at lower temperatures. However, all sites are poorly defined, i.e., a lot of disorder is seen in the nearest neighbour shells of iron.

Crystalline phases appear for sample annealed at 623 K as the early nucleation of the phosphide phase is unseen directly by the Mössbauer spectroscopy. The iron could be found in the (Ni, Fe, Cu)$_3$P phase (see, the following sub-section), (Ni, Fe, Cu)-FCC phase [18,21,22] and in some remnants of the amorphous FCC-like phase. The crystalline (Ni, Fe, Cu)-FCC phase is ferromagnetic in contrast to the phosphide phase—at room temperature. A similar situation is observed for the sample annealed at 648 K, however a contribution from the amorphous phase is lowered in comparison with the previous sample (see, Table 1).

On the other hand, one can see some increase of the signal due to the (Ni, Fe, Cu)$_3$P phase, and some ordering of the (Ni, Fe, Cu)-FCC phase seen as the increase of the average hyperfine field on the iron nucleus. The latter ordering is probably due to the phosphorus transfer from the FCC phase to the phosphide. No amorphous phase containing iron is found for the sample annealed at 673 K. The FCC phase of this sample is further depleted in phosphorus, and some iron transfer is observed from the FCC phase to the (Ni, Fe, Cu)$_3$P phase. The spectrum of the sample annealed at 773 K is similar to the previous one. Some iron transfer from the FCC phase to the (Ni, Fe, Cu)$_3$P phase is still seen. It is likely that the sample reaches stability upon annealing for 1 h at about 773 K. The iron in the (Ni, Fe, Cu)-FCC phase has higher average isomer shift than in either nickel [18], copper [23] or nickel copper alloys [24]. This is an indication of the decreased electron density caused by the remnants of the phosphorus in this phase. A distribution of the hyperfine magnetic fields on the iron nuclei (see, Fig. 4) gets narrower with the increasing annealing temperature due to the sample ordering. The average field tends to the field in the pure nickel, the latter being 26.75 T [18,25] upon increasing the annealing temperature. Distributions of the magnetic field and shift (local electron density) are due to various configurations around the iron atom in the (Ni, Fe, Cu)-FCC phase. Neighbours beyond the third co-ordination shell at most have no effect on the distributions except average values in the most of the metallic systems [26].

The phosphide (Ni, Fe, Cu)$_3$P has been found (see, the following sub-section) iso-structural with either Fe$_3$P or Ni$_3$P compounds, the latter compounds crystallising with the $I\bar{4}$ space group belonging to the tetragonal system [27]. There are eight molecules per chemical unit cell with three different crystallographic sites (8 g) occupied by metal atoms, and a single phosphorus crystallographic site (8 g). All these positions are general Wyckoff positions. The Fe$_3$P compound is magnetically ordered at room temperature with the significant net magnetic moment per unit cell. On the other hand, the Ni$_3$P compound
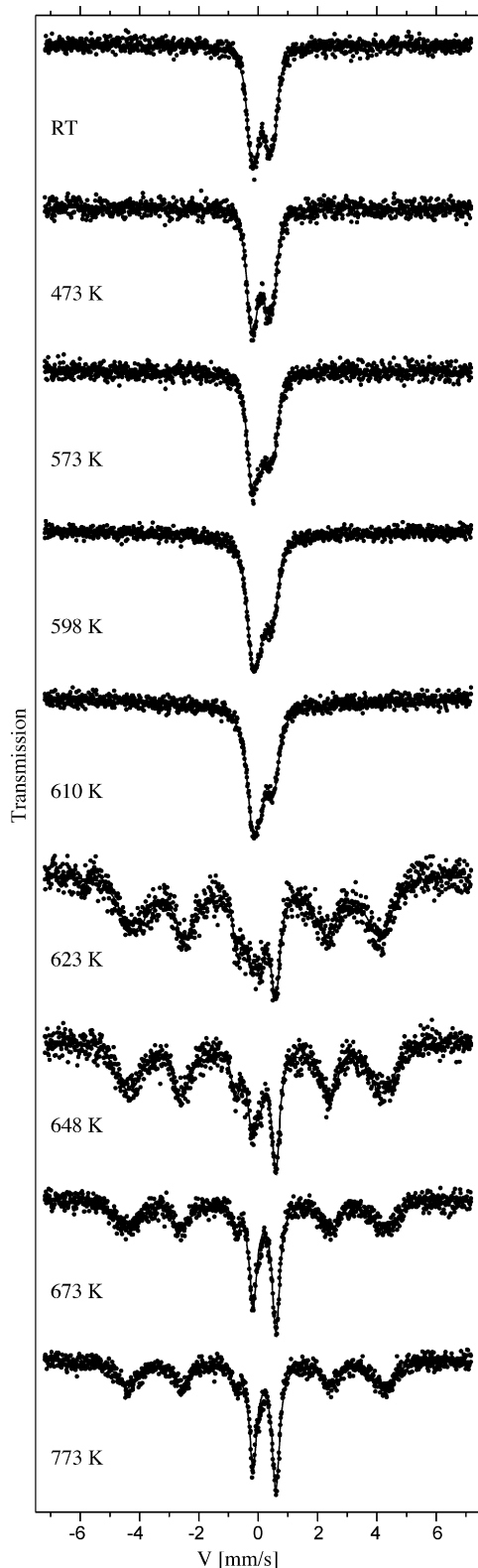
Fig. 3. Mössbauer spectra are shown vs. annealing temperature. The spectra were collected for the source and absorbers kept at room temperature. The symbol V stands for the relative velocity along the radiation beam between source and the absorber. A positive velocity corresponds to the source approaching the absorber.
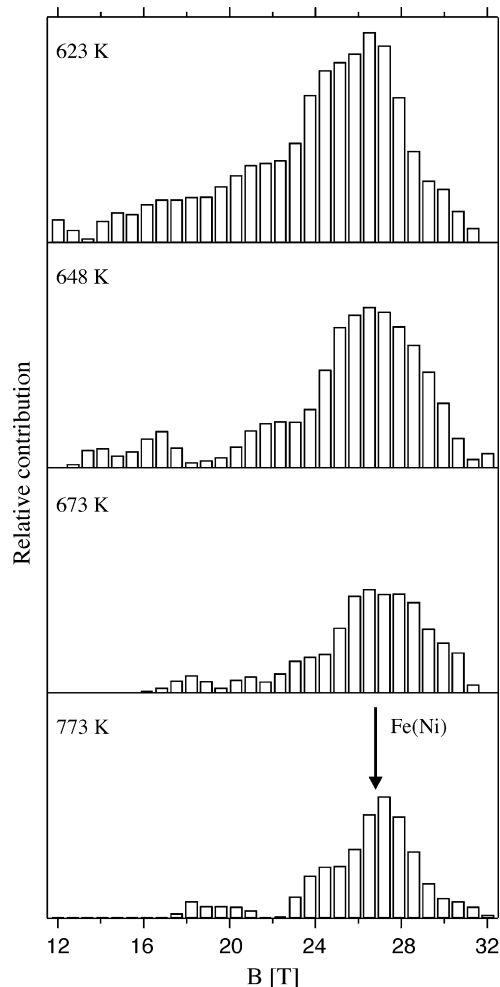

Fig. 4. Distributions of the hyperfine fields are shown for various annealing temperatures. Distributions are normalised to the amount of the magnetically ordered phase. The arrow shows the hyperfine field for the isolated iron impurity in nickel at room temperature. The symbol B stands for the hyperfine effective magnetic field on the iron at room temperature.

remains paramagnetic at room temperature. The Mössbauer spectroscopy revealed six iron environments in the magnetically ordered Fe_3P [28,29]. This is an indication of the quite complex magnetic structure as each of the crystallographic metal sites is split into two inequivalent sites upon magnetic ordering. On the other hand, the neutron diffraction data indicate only three different magnetic moments of iron [28]. All six iron sites exhibit some electric quadrupole interactions [28,29]. However, some data obtained on Fe_3P above the magnetic transition point indicate that these interactions are almost negligible at high temperature [30].

This unusual behaviour is some indication of the unquenched electron orbital magnetic moment contribution to the hyperfine magnetic field and the electric field gradient tensor on the iron nuclei. The mixed phosphide investigated here remains paramagnetic at room temperature due to the high content of nickel and probably copper as well. We have found a single iron site with the almost the same isomer shift at room temperature (see, Table 1) as the room temperature shift (0.34 mm/s) on the iron

surrounded by four phosphorus atoms in the Fe_3P phosphide [28]. Hence, it seems that iron atoms substitute nickel (and probably copper as well) almost exclusively on this site—called further site II [28,29]. The electric quadrupole interactions measured on the site II of the magnetically ordered Fe_3P at room temperature show either -0.12 mm/s or -0.10 mm/s splitting depending upon the magnetic site. We have found much larger absolute value of the splitting (see, Table 1). The discrepancy is probably due to the fact that the appropriate hyperfine fields in the Fe_3P phosphide point close to the magic directions in the respective electric field gradient reference frames. One has to note that the corresponding fields amount to either 18.0 T or 17.0 T, respectively [28]. Under such circumstances the electric quadrupole Hamiltonians exhibit themselves as the first order perturbations to the respective dipolar magnetic interactions.

3.4. X-ray diffraction

X-ray patterns versus annealing temperature were obtained at room temperature with the help of the DRON-3 powder diffractometer using Cu Kα radiation filtered by the LiF linearly focusing monochromator on the detector side. The scattering surface of the annealed ribbons was the one exposed to the spinning wheel surface. The sample as cast was investigated from both sides. The scattering angle 2θ was varied with the constant step of $0.05°$. Scans were performed in the θ–2θ mode. The sample annealed at 773 K has been investigated in detail at room temperature applying Cu Kα radiation filtered on the detector side with the help of the pyrolytic graphite monochromator. The scattering surface was again the surface in contact with the spinning wheel.
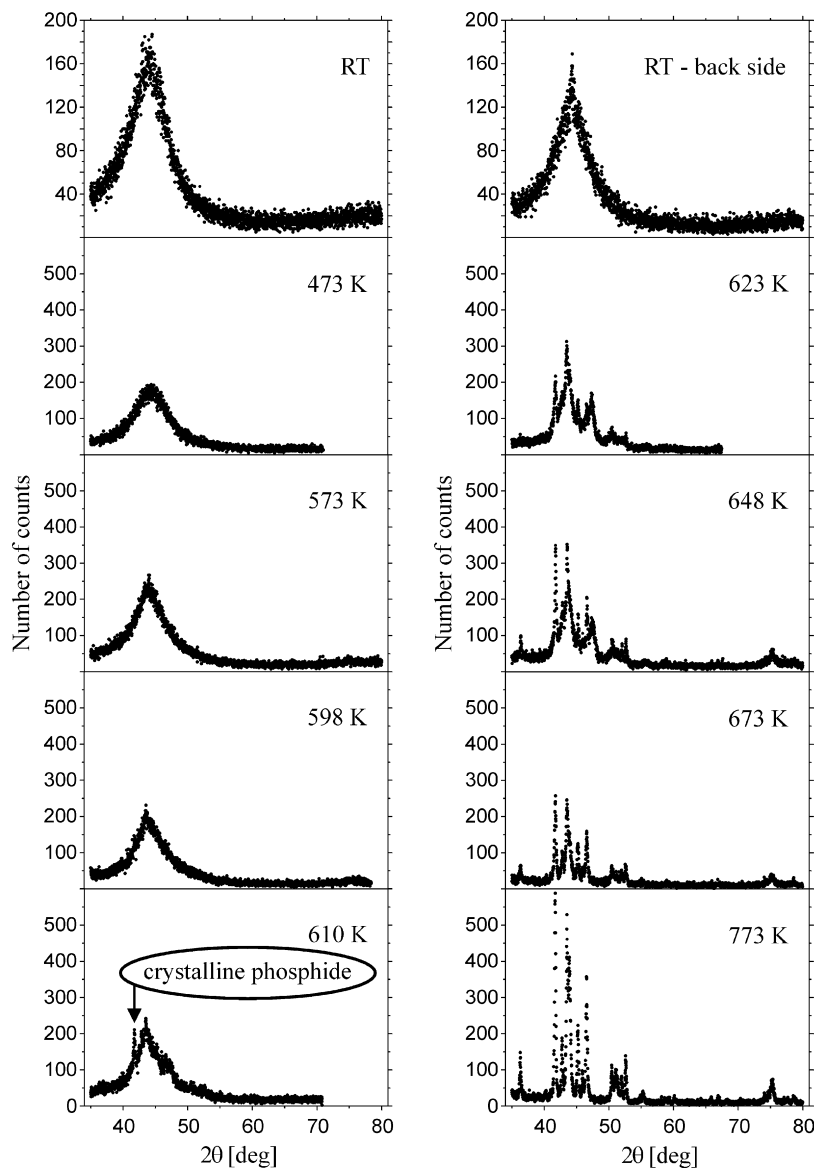

Fig. 5. X-ray patterns collected at room temperature are shown vs. annealing temperature. The symbol RT-back side denotes the sample as cast with the scattering surface being the surface opposite to the surface in touch with the spinning wheel. The symbol RT denotes the sample as cast.

Table 2
Essential crystal parameters derived from the X-ray diffraction pattern obtained at room temperature on the sample annealed at 773 K

FCC phase	Phosphide phase			
	$a = 0.89645(9)$ [nm] $c = 0.43984(5)$ [nm]			
	Atomic positions	x	y	z
$a = 0.35734(6)$ [nm]	M(I) (2P)	0.0743(14)	0.1091(13)	0.2400(51)
contribution: 23.1	M(II) (4P)	0.3611(12)	0.0353(16)	0.9735(52)
(1.2) [%]	M(III) (3P)	0.1722(13)	0.2175(11)	0.7530(56)
	P	0.2954(19)	0.0465(21)	0.4861(56)

The FCC phase has $Fm\bar{3}m$ space group, while the phosphide phase has $I\bar{4}$ space group. The symbol M denotes Ni, Fe or Cu. Mössbauer data suggest that Fe is present almost solely on the site II. Symbols (2P), (4P) and (3P) indicate the number of P atoms as the nearest neighbours (at distances ranging from 0.14 nm to 0.22 nm, the second neighbours are distant from 0.36 nm to 0.39 nm) of the respective metal atom.

It is obvious that the sample as cast is amorphous across the whole ribbon thickness. The long-range order starts to appear in the samples at about 623 K in accordance with the results obtained by the Mössbauer spectroscopy. For details see Fig. 5. It is interesting to note that the crystallisation starts as the nucleation of the phosphide phase.

Two phases were found, i.e., the (Ni, Fe, Cu)-FCC phase and the (Ni, Fe, Cu)$_3$P phosphide. Essential results are summarised in Table 2. The lattice constant of the FCC phase is slightly bigger than the lattice constant of the pure nickel ($a = 0.35241$ nm at room temperature for Ni). Such behaviour is expected due to the presence of iron and copper in this phase. Some interstitial phosphorus is likely to be present as well. Lattice constants for Fe$_3$P at room temperature are $a = 0.9107$ nm and $c = 0.446$ nm, while the same lattice constants for Ni$_3$P are $a = 0.895$ nm and $c = 0.439$ nm at room temperature. Therefore, the phosphide M$_3$P (M = Ni, Fe, Cu) obtained in the present research is very similar to the Ni$_3$P compound with slightly enlarged lattice constants due to the presence of iron and probably copper as well. A contribution due to the FCC phase cannot be determined very
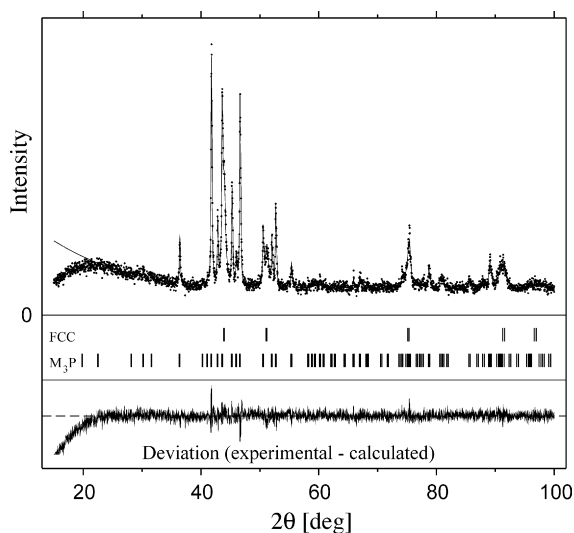

Fig. 6. The X-ray pattern collected at room temperature on the sample annealed at the temperature of 773 K for 1 h. The scattering surface was the surface exposed to the spinning wheel. This pattern was used to derive data of the Table 2. Vertical bars show positions of the reflections belonging to the respective phases. The solid line is the result of the Rietveld fit to the data.

accurately, however it indicates that the phase separation and crystallisation process is close to completion. The X-ray pattern used to derive data of the Table 2 is shown in Fig. 6.

One can conclude taking into account the Mössbauer and the X-ray diffraction results (see, Tables 1 and 2) that iron is almost evenly distributed among the FCC phase and the site II of the phosphide upon completion of the phase separation and crystallisation. Some copper has to be transferred from the FCC phase to the metal sites in the phosphide as can be seen from the respective hyperfine fields distribution shown in Fig. 4 for the sample annealed at the highest temperature. However, no quantitative statement could be made about the copper distribution among the various phases and sites without performing detailed studies by some microscopic method sensitive to the copper atom local environment like, e.g. the nuclear magnetic resonance.

4. Conclusions

1. Melt spinning technique provides sufficient cooling conditions for amorphisation of the alloy—SAED pattern exhibits diffuse rings and X-ray diffraction patterns present very broad diffusive ring typical for metallic glasses with virtually no order beyond the nearest neighbours.
2. Annealing at the temperature range 473–598 K gives contribution from the high symmetry site at the cost of the sites having phosphorus as the nearest neighbours. Particularly the site with less phosphorus as the nearest neighbours transforms into the FCC-like site.
3. The sample annealed at 610 K is characterised by merging of two iron sites having phosphorus as the nearest neighbours. A transformation proceeds towards (Ni, Fe, Cu)P-like site. A contribution from the FCC-like sites is increased in comparison with samples annealed at lower temperatures. A substantial disorder in the nearest neighbour shells of iron brings about poor definition of all sites.
4. After 1 h annealing, crystallisation of the alloy can be observed at isochronal cycles performed at 623 K, 648 K, 673 K and 773 K. For increasing temperature one can observe progressive formation of the (Ni, Fe, Cu)$_3$P phase and (Ni, Fe, Cu)-FCC phase at the cost of the amorphous regions of the samples. The iron could be found in the (Ni, Fe, Cu)$_3$P phase, (Ni, Fe, Cu)-FCC phase and in some remnants of the

amorphous FCC-like phase. After the thermal cycles, at room temperature, the crystalline (Ni, Fe, Cu)-FCC phase is ferromagnetic in contrast to the phosphide phase. Furthermore, depletion of the FCC phase in phosphorus is observed during the crystallisation and some iron transfer is observed from the FCC phase to the $(Ni, Fe, Cu)_3P$ phase.

5. The phosphide $(Ni, Fe, Cu)_3P$ formed during the crystallisation is iso-structural with either Fe_3P or Ni_3P compounds and can be classified with the $I\bar{4}$ space group belonging to the tetragonal system. Crystallisation begins as the nucleation of the phosphide phase. The first crystalline nuclei of the phosphide appear already upon annealing for 1 h at 610 K.

Acknowledgement

References

[1] A. Inoue, T. Nakamura, N. Nishiyama, T. Masumoto, Mater. Trans. JIM 33 (1990) 937.
[2] A. Peker, W.L. Johnson, Appl. Phys. Lett. 63 (1993) 2342.
[3] Y. He, R.B. Schwarz, J.I. Archuleta, Appl. Phys. Lett. 69 (1996) 1861.
[4] K. Russew, B.J. Zappel, F. Sommer, Scripta Metall. Mater. 32 (1995) 271.
[5] Q. Wang, J.J. Blandin, M. Suery, J.M. Pelletier, Mater. Res. Soc. Symp. Proc. 754 (2003) 315.
[6] Y. Kawamura, T. Shibata, A. Inoue, T. Masumoto, Acta Mater. 46 (1998) 253.
[7] S.N. Nathaudhu, J.T. Im, R.E. Barber, I.E. Anderson, I. Karaman, K.T. Hartwig, Mat. Res. Soc. Symp. Proc. 754 (2003) 191.
[8] Z.P. Lu, T.T. Goh, Y. Li, S.C. Ng, Acta Mater. 47 (7) (1999) 2215.
[9] G.J. Fan, W. Loeser, S. Roth, J. Eckert, L. Schultz, J. Mater. Res. 15 (7) (2000) 1556.
[10] C.C. Hays, J. Schroers, W.L. Johnson, Appl. Phys. Lett. 79 (11) (2001) 1605.
[11] Y. Zhang, D.Q. Zhao, B.C. Wei, P. Wen, M.X. Pan, W.H. Wang, J. Mater. Res. 16 (6) (2001) 1675.
[12] R. Willnecker, K. Wittmann, G.P. Görler, J. Non-Cryst. Solids 156–158 (1993) 450.
[13] A. Inoue, N. Nishiyama, Mater. Sci. Eng. A226–A228 (1997) 401.
[14] Z.P. Lu, Y. Li, S.C. Ng, J. Non-Cryst. Solids 270 (2000) 103.
[15] P. Villars, A. Prince, H. Okamoto, Handbook of Ternary Alloy Phase Diagrams, vols. 8 and 10, The Materials Information Society, ASM International, 1995.
[16] K. Ziewiec, P. Olszewski, R. Gajerski, S. Kąc, A. Ziewiec, Z. Kędzierski, J. Non-Cryst. Solids 343 (2004) 150.
[17] R. Górnicki, RENON, http://www.renon.strefa.pl.
[18] G. Longworth, T.E. Cranshaw, J. Magn. Magn. Mater. 30 (1983) 371.
[19] L. Häggström, A. Narayanasamy, J. Magn. Magn. Mater. 30 (1982) 249.
[20] V.V. Nemoshkalenko, N.A. Tomashevskii, V.B. Chernogorenko, L.Ya. Solomatina, Poroshkovaya Metall. 21 (1982) 57.
[21] L. Larsen, H. Roy-Poulsen, N.O. Roy-Poulsen, L. Vistisen, J.M. Knudsen, Phys. Rev. Lett. 48 (1982) 1054.
[22] A.D. Lehlooh, S.H. Mahmood, Hyperfine Interact. 139–140 (2002) 387.
[23] S.M. Quaim, Proc. Phys. Soc. 90 (1967) 1065.
[24] R.C. Reno, L.J. Swartzendruber, Phys. Rev. Lett. 29 (1972) 712.
[25] C. Hohenemser, R. Reno, H.C. Benski, J. Lehr, Phys. Rev. 184 (1969) 298.
[26] A. Błachowski, K. Ruebenbauer, J. Żukrowski, Phys. Scr. 70 (2004) 368.
[27] S. Rundqvist, E. Hassler, L. Lundvik, Acta Chem. Scand. 16 (1962) 242.
[28] Yu.N. Vorobyev, Ye P. Yelsukov, Phys. Stat. Sol. (b) 205 (1998) R13.
[29] E.J. Lisher, C. Wilkinson, T. Ericsson, L. Häggström, L. Lundgren, R. Wäppling, J. Phys. C: Solid State Phys. 7 (1994) 1344.
[30] R.E. Bailey, J.F. Duncan, Inorg. Chem. 6 (1967) 1444.